NASA/TM—2005-213800 ARL–MR–0628

NASA Glenn Research Center Program in High Power Density Motors for Aeropropulsion

Gerald V. Brown
Glenn Research Center, Cleveland, Ohio

Albert F. Kascak
U.S. Army Research Laboratory, Glenn Research Center, Cleveland, Ohio

Ben Ebihara
University of Toledo, Toledo, Ohio

Dexter Johnson and Benjamin Choi
Glenn Research Center, Cleveland, Ohio

Mark Siebert and Carl Buccieri
University of Toledo, Toledo, Ohio

December 2005

The NASA STI Program Office . . . in Profile

Since its founding, NASA has been dedicated to the advancement of aeronautics and space science. The NASA Scientific and Technical Information (STI) Program Office plays a key part in helping NASA maintain this important role.

The NASA STI Program Office is operated by Langley Research Center, the Lead Center for NASA's scientific and technical information. The NASA STI Program Office provides access to the NASA STI Database, the largest collection of aeronautical and space science STI in the world. The Program Office is also NASA's institutional mechanism for disseminating the results of its research and development activities. These results are published by NASA in the NASA STI Report Series, which includes the following report types:

- TECHNICAL PUBLICATION. Reports of completed research or a major significant phase of research that present the results of NASA programs and include extensive data or theoretical analysis. Includes compilations of significant scientific and technical data and information deemed to be of continuing reference value. NASA's counterpart of peer-reviewed formal professional papers but has less stringent limitations on manuscript length and extent of graphic presentations.

- TECHNICAL MEMORANDUM. Scientific and technical findings that are preliminary or of specialized interest, e.g., quick release reports, working papers, and bibliographies that contain minimal annotation. Does not contain extensive analysis.

- CONTRACTOR REPORT. Scientific and technical findings by NASA-sponsored contractors and grantees.

- CONFERENCE PUBLICATION. Collected papers from scientific and technical conferences, symposia, seminars, or other meetings sponsored or cosponsored by NASA.

- SPECIAL PUBLICATION. Scientific, technical, or historical information from NASA programs, projects, and missions, often concerned with subjects having substantial public interest.

- TECHNICAL TRANSLATION. English-language translations of foreign scientific and technical material pertinent to NASA's mission.

Specialized services that complement the STI Program Office's diverse offerings include creating custom thesauri, building customized databases, organizing and publishing research results . . . even providing videos.

For more information about the NASA STI Program Office, see the following:

- Access the NASA STI Program Home Page at ***http://www.sti.nasa.gov***

- E-mail your question via the Internet to help@sti.nasa.gov

- Fax your question to the NASA Access Help Desk at 301–621–0134

- Telephone the NASA Access Help Desk at 301–621–0390

- Write to:
  NASA Access Help Desk
  NASA Center for AeroSpace Information
  7121 Standard Drive
  Hanover, MD 21076

NASA/TM—2005-213800 ARL–MR–0628

NASA Glenn Research Center Program in High Power Density Motors for Aeropropulsion

Gerald V. Brown
Glenn Research Center, Cleveland, Ohio

Albert F. Kascak
U.S. Army Research Laboratory, Glenn Research Center, Cleveland, Ohio

Ben Ebihara
University of Toledo, Toledo, Ohio

Dexter Johnson and Benjamin Choi
Glenn Research Center, Cleveland, Ohio

Mark Siebert and Carl Buccieri
University of Toledo, Toledo, Ohio

National Aeronautics and
Space Administration

Glenn Research Center

December 2005

Acknowledgments

Dr. Timothy Krantz developed the gear-box data and correlation. Jeffrey Trudell performed stress analysis for the switched reluctance motor and the tip-drive rig. This work was sponsored by the Alternate Energy Foundation Technologies Sub-Project of the Low Emissions Alternative Power Project at NASA Glenn Research Center, David Ercegovic, Leo Burkardt, and Kim Pham, project managers.

This work was sponsored by the Low Emissions Alternative Power Project of the Vehicle Systems Program at the NASA Glenn Research Center.

Available from

NASA Center for Aerospace Information
7121 Standard Drive
Hanover, MD 21076

National Technical Information Service
5285 Port Royal Road
Springfield, VA 22100

Available electronically at http://gltrs.grc.nasa.gov

NASA Glenn Research Center Program in High Power Density Motors for Aeropropulsion

Gerald V. Brown
National Aeronautics and Space Administration
Glenn Research Center
Cleveland, Ohio 44135

Albert F. Kascak
U.S. Army Research Laboratory
Glenn Research Center
Cleveland, Ohio 44135

Ben Ebihara
University of Toledo
Toledo, Ohio 43606

Dexter Johnson and Benjamin Choi
National Aeronautics and Space Administration
Glenn Research Center
Cleveland, Ohio 44135

Mark Siebert and Carl Buccieri
University of Toledo
Toledo, Ohio 43606

Abstract

Electric drive of transport-sized aircraft propulsors, with electric power generated by fuel cells or turbo-generators, will require electric motors with much higher power density than conventional room-temperature machines. Cryogenic cooling of the motor windings by the liquid hydrogen fuel offers a possible solution, enabling motors with higher power density than turbine engines. Some context on weights of various systems, which is required to assess the problem, is presented. This context includes a survey of turbine engine weights over a considerable size range, a correlation of gear box weights and some examples of conventional and advanced electric motor weights. The NASA Glenn Research Center program for high power density motors is outlined and some technical results to date are presented. These results include current densities of 5,000 A/cm^2 current density achieved in cryogenic coils, finite element predictions compared to measurements of torque production in a switched reluctance motor, and initial tests of a cryogenic switched reluctance motor.

Introduction

Pollution-free flight is one of NASA's goals for the 21st Century. One method of approaching that goal is hydrogen-fueled aircraft that use fuel cells or turbo-generators to develop electric power that can drive electric motors that turn the aircraft's propulsive fans or propellers ("propulsors"). Hydrogen fuel would likely be carried as a liquid, stored in tanks at its boiling point of 20.3 K (–423 ºF). Figure 1 compares a conventional propulsor drive system with an electric drive system with electric power shown produced by fuel cells, turbo-generators or, futuristically, beamed from earth or space.

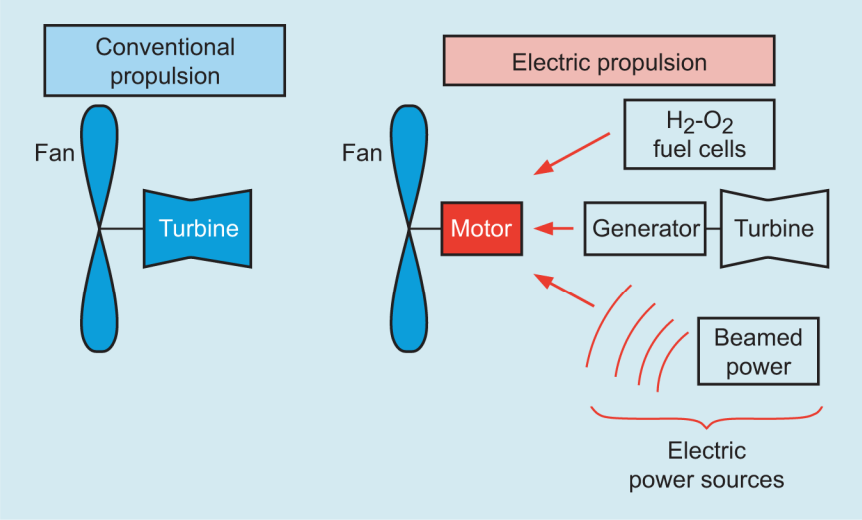

Figure 1.—Comparison of conventional and electric propulsion systems.

Some benefits and possible technical challenges of electric drive are listed in table I.

Table I.

Advantages	Challenges
Cross coupling of prime movers and propulsors	Potentially heavier if many components not redesigned
Symmetrical thrust maintained with partial prime mover failure	Possibly heavy electric power bus leads
Decoupling of rpm and torque capability	Possibly heavy power conditioning
Possible prime mover shut-off during cruise	

Conventional electric motors, however, are far too heavy (for a given horsepower) to use on aircraft, as illustrated in figure 2.

Fortunately the liquid hydrogen fuel can provide essentially free refrigeration that can be used to cool the windings of motors before the hydrogen is used for fuel. Either High Temperature Superconductors (HTS) or high purity metals such as copper or aluminum may be used in the motor windings. Superconductors have essentially zero electrical resistance to steady current. The electrical resistance of high purity aluminum or copper near liquid hydrogen temperature can be $1/100^{th}$ or less of the room temperature resistance. These conductors could provide higher motor efficiency than normal room-temperature motors achieve. But much more importantly, these conductors can carry ten to a hundred times more current density than copper conductors do in normal motors operating at room temperature (refs. 1 to 5). This is a consequence of the low (or zero) resistance and of good heat transfer coefficients to boiling LH_2 or to flowing supercritical H_2. Thus the conductors can produce higher magnetic field strengths and consequently higher motor torque and power. Pictorial comparisons of each type of conductor with room-temperature conductors are shown in figure 3.

Designs, analysis and actual cryogenic motor tests show that such cryogenic motors could produce three or more times as much power per unit weight as turbine engines can, whereas conventional motors produce only 1/5 as much power per weight as turbine engines.

A rough understanding of why conventional motors are inferior in power density to turbine engines, and why cryogenic motors can be better, is provided by a look at the peak energy density or "pressure" in the machines. We postulate that energy density or pressure is a rough indication of the ability to do work (as gas pressure does work on turbine blades in a turbine engine). A magnetic energy density or pressure P (in atmospheres) can be defined in terms of the magnetic field strength B (in Teslas) by $P \approx 4\ B^2$. By using this equation, we see that the 25 to 40 atmospheres in the core of a turbine engine is much greater than the 10 or so atmospheres of "pressure" in a conventional electric machine operating at 1.6 Teslas in its working air gap. A cryogenic motor operating at 5 Teslas, on the other hand, would have an energy

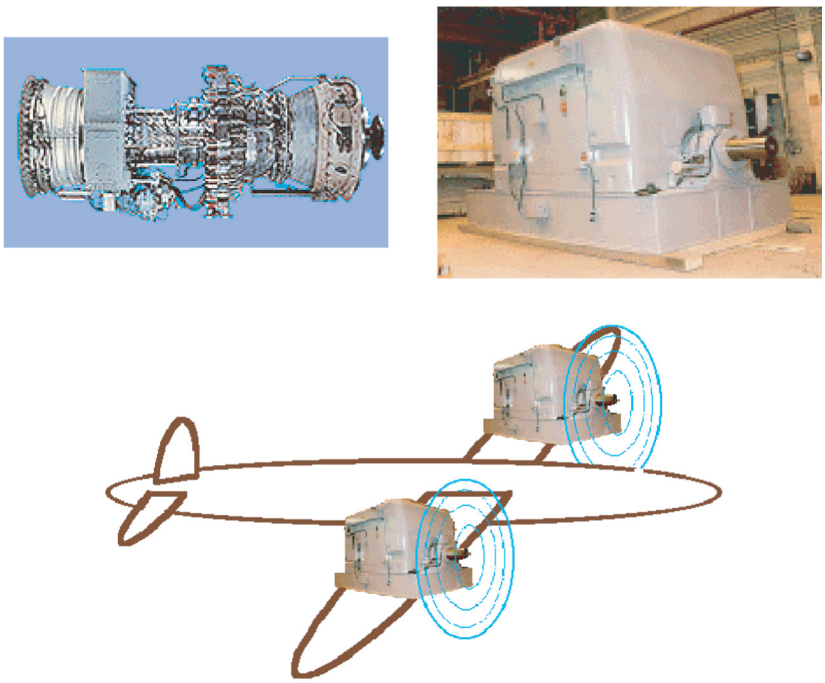

Figure 2.—A large turbine engine (upper left) is more compact and lighter than a conventional industrial electric motor of the same horsepower (upper right). A large aircraft powered by conventional electric motors would be ungainly, as indicated whimsically (below).

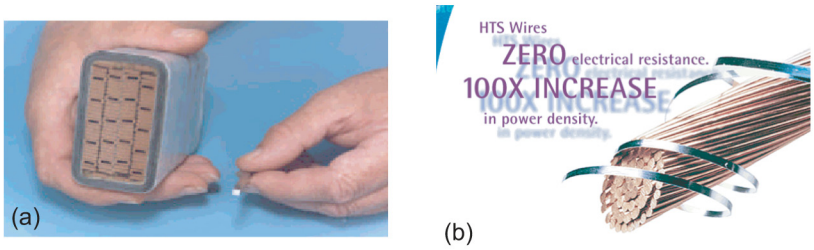

Figure 3.—Comparisons of high purity aluminum conductor and superconducting tape with normal room-temperature copper conductors of similar current-carrying capacity. (a) High purity aluminum conductor (for use in liquid hydrogen), compared to industrial motor conductor. (b) Superconducting tape compared to copper cable.

density or pressure of 100 atmospheres in its working gap, a value far superior to existing turbine engine values. (In making this rough plausibility argument, we ignore the relative volumes in which these energy densities exist.) The comparison is shown graphically in figure 4.

These relative energy densities are reflected in a comparison of typical power densities in various motors and engines, as shown in figure 5. But it must be emphasized that, although cryogenic motors look better than turbine engines in this comparison, turbine engines are prime movers, developing shaft power from fuel, whereas motors are not prime movers. A complete comparison requires the addition to the motor weight of the weight of components that produce the electric power from fuel and any electric power conditioning electronics.

Two of the highest density electric machines so far demonstrated are an axial-gap permanent magnet machine developed for the Army Tank-Automotive Command (TACOM) and a cryogenic synchronous generator developed for the Air Force. (We make no distinction between motors and generators.) Figure 6 pictures these machines. The TACOM machine, which operates at room temperature and was developed

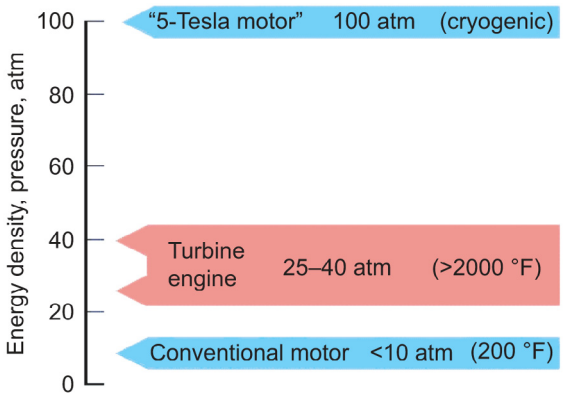

Figure 4.—Comparison of energy density (or pressure) in turbine engines and motors.

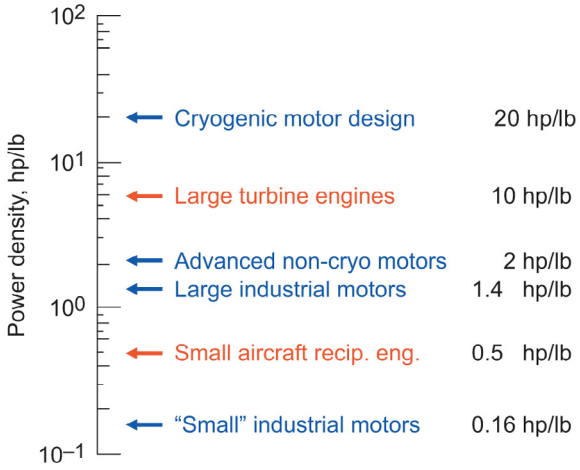

Figure 5.—Power density comparison of engines and motors.

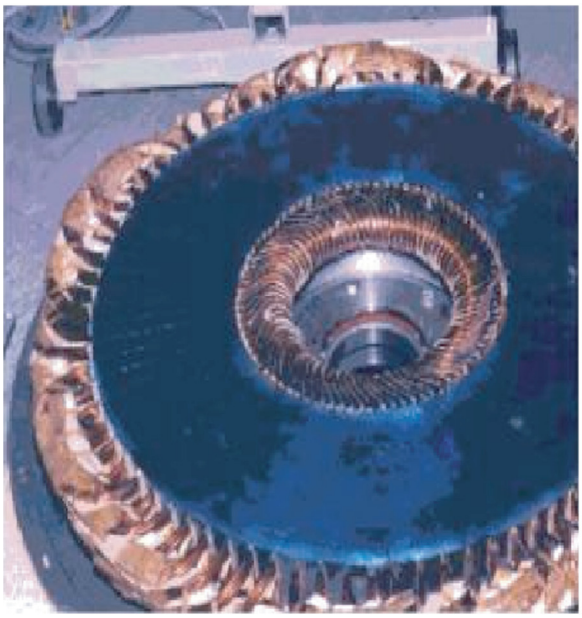

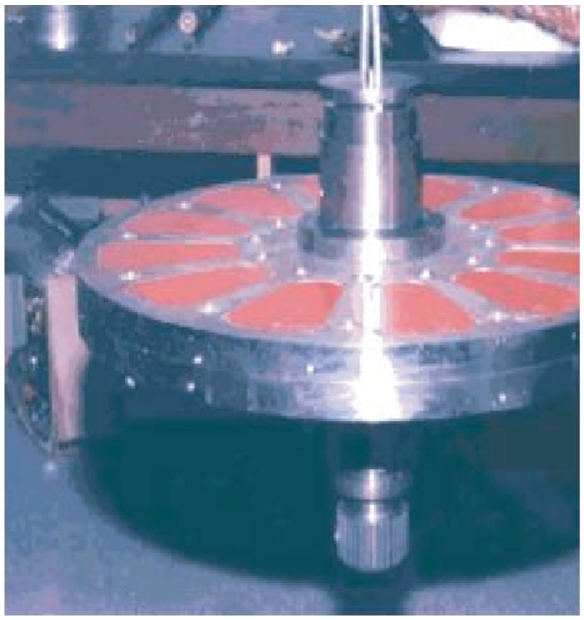

Figure 6.—TACOM axial-gap permanent magnet motor for ground-vehicle propulsion (top, stator on left, rotor on right) and Air Force cryogenic generator (below, assembled on left, stator on right).

to propel ground vehicles, has a power density of around 2 hp/lb (3.3 kW/kg) (ref. 6). The Air Force cryogenic generator was operated at open circuit and short circuit conditions but was not run under full power conditions. It was designed for about 600 kW, but the short circuit and open circuit test results indicated that it could handle 1MW continuous (ref. 7). At that power level it would produce about 6 hp/lb (~10 kW/kg).

Weight Comparisons of Motors, Engines, Fuel Cells and Gearboxes

To help determine what improvements may be needed in various electric aircraft drive components, a number of data sets and trend lines have been developed. Plots of the weights of a number of motors and engines and some trend lines are shown in the next several figures.

Comparing a turbofan engine with an electric-motor-driven-fan system requires some decisions on how much power the motor must produce, as well as how much of the turbine engine is actually replaced. We start with published (refs. 8 to 11) and proprietary data on turbofan engine weight and thrust. Data is shown in figure 7(a). The thrust shown is thrust at sea-level static take-off. Note that the power-law-fit exponent is about 0.9, indicating some economy of scale.

The published weights of turbine engines usually include the "propulsor," that is, the propulsive fan and related components such as the fan frame, brackets, supports, exit guide vanes and containment. These propulsor components would all be required with an electric motor drive. Our first step in making an appropriate comparison of motors and turbofan engines, therefore, is to subtract the propulsor weight from the total weight of a turbofan engine. We have some proprietary data for actual propulsor weights for large turbofan engines. The average fraction of total engine weight represented by the propulsor components is 30 percent. This factor was used to estimate the propulsor weight for all the "mid-range" engines in our survey, even though it would vary with bypass ratio and other variables. Actual values are used for the large engines for which we have data.

A second issue is that the power delivered to the propulsive fan, which a motor would have to supply, is not typically published. Instead, the total turbofan engine thrust T_{tot} (sea-level static take-off thrust) is published. This total thrust is the sum of the thrust from the fan and the thrust from the jet. From some proprietary data we have derived a typical relation, for engines between 15,000 and 100,000 lb thrust, that the power $P_{fan,rot}$ in horsepower, delivered to the fan through the fan shaft at take-off rotation (mach 0.25), is 0.97 times the total engine sea-level static thrust in pounds.

$$P_{fan,rot} = 0.97 * T_{tot} \ (T_{tot} \text{ in lb}, P_{fan} \text{ in hp})$$

Even though the factor would vary somewhat from 0.97 with bypass ratio and other variables, we have used that single value for all the engines in our survey.

The remaining issue is how to deal with the jet thrust of a turbine engine, which does not exist for an electric motor driven fan. If an electric motor were to drive the fan used in a particular turbofan engine (at the same speed and with the same torque), the resulting thrust would be lower than the total thrust of the turbofan engine including its jet. We have chosen a factor of 0.8 to estimate fan thrust T_{fan} from total turbofan engine thrust T_{tot}, i.e.,

$$T_{fan} = 0.8 * T_{tot}.$$

Although the factor would be expected to vary from 0.8 with bypass ratio and other variables, we have used it for all the engines in our survey. Hence we will plot what we consider a "replacement effective power output" of the turbofan engine which is 1.25 times the fan horsepower. This power reasonably represents the power that a motor would have to produce to give the same thrust as a turbine engine. This would be accomplished with a somewhat larger fan than the turbine engine used. Figure 7(b) presents the weights (less propulsor weights) of the turbine engines versus their effective replacement power output at take-off rotation.

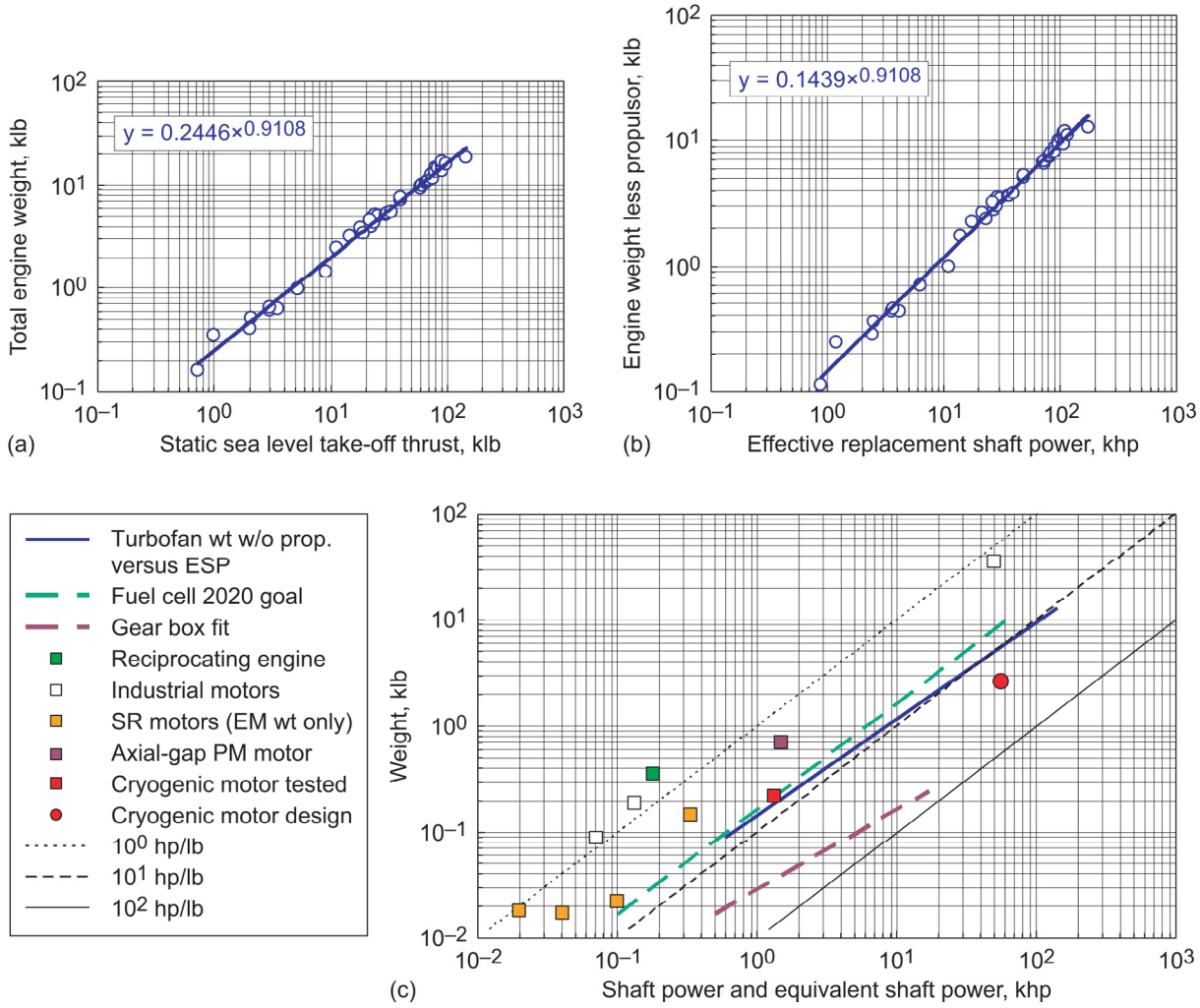

Figure 7.—(a) Raw data on turbine engine thrust and weight with power-law trend-line. (b) Turbofan engine weight (less propulsor weight) as a function of effective replacement shaft power. (c) Weight versus power for a number of systems.

The power-law fit of the data in figure 7(b) is used in the next graph to represent the performance level that motors must match or exceed. Of course, the weight of the source of electric power and any power electronics must be added to motor weight for comparison with the turbine engine.

A number of systems are compared in figure 7(c) on the basis of weight plotted versus power. The dark blue line is the power law fit to the weight versus effective power from the previous figure. The dashed green line shows the weight of fuel cell systems (stack plus accessories, not including output power conditioning), as represented by the 2020 goal of 6 hp/lb (10 kW/kg). Present automotive-derivative fuel-cell technology produces on the order of 0.4 hp/lb (0.66 kW/kg), and government and industry laboratory demonstrations are indicating about 1.0 hp/lb (1.6 kW/kg) (ref. 12). If the 2020 goal is achieved, it can be seen that fuel cell weight will still exceed that of turbine engines. Hence fuel cells may likely be used only in some kind of hybrid combination. Their projected higher efficiency (~60 percent versus ~40 percent for turbine engines) may at least allow their use for cruise, with more conventional power augmentation for take-off. However, fuel cells are already lighter than reciprocating engines for small aircraft, one of which is plotted as a green square at 180 hp and 360 lb. Early electric flight demonstrations on small aircraft appear to be possible, even with near-term fuel-cell technology.

The dashed purple line in figure 7(c) is an approximation to the weight of a gearbox that might be used between a motor and a propulsor to allow different shaft speeds in the two components. This line, derived from a gearbox weight correlation discussed below, is for a three-to-one reduction in shaft speed from motor to propulsor. (Note that propulsor tip speed is limited to mach 1.5 or less, or even to only mach 0.8 for low noise propulsors, limiting large diameter fans to 2000 rpm or less.) Most motors would develop better power density at perhaps 6000 rpm, or even much higher. Figure 7(c) shows that the weight of a gearbox would not be a significant weight penalty, since a gearbox weighs much less than any cryogenic motors we can envision at present.

A number of motor weights are shown in figure 7(c). A typical large industrial motor, shown at 50,000 hp and 36,000 lb, weighs about seven times as much as a turbine engine producing the same thrust, as indicated by the turbine engine trend line. The two smaller commercial motors shown have superior power density to the reciprocating engine. Note that the projected fuel cell weights are an order of magnitude lower than both the reciprocating engine and the industrial motors shown for that power output range.

The axial-gap permanent-magnet motor built for TACOM, shown in figure 7(c) at 1500 hp and 700 lb, though about 3.5 times as heavy as the turbine engine for the same power, is the best room-temperature motor, in terms of power density, for which we have data above 100 hp.

Switched reluctance motors and generators appear to offer the best specific power levels in the power output range below 300 or 400 hp, and several advanced Integrated Starter/Generators (ISG's) and Auxiliary Power Units (APU's) have been designed and tested. Data for three of these are shown in figure 7(c). The point at 40 hp and 18 lb (electromagnetic weight only) is from reference 13. The point at 100 hp and 22 lb (electromagnetic weight only) is from reference 14, and if a factor of 1.5 is used to convert from electromagnetic weight to total weight, it would correspond to a specific power of 3 hp/lb (5 kW/kg). This is the best non-cryogenic motor in terms of power density in any power range of which we are presently aware.

Cryogenic motors, as indicated above, have the greatest specific power capability. Only one cryogenic electric machine known to us, the Air Force generator, was designed with a flight-weight objective. This is the 220 lb Air Force synchronous machine pictured in figure 6. At its potential power capability of 1 MW (ref. 6), this machine would have the highest power density of any actually built electrical machine known to us. (It is shown in figure 7(c) at 220 lb and the machine's indicated power potential of 1 MW (1340 hp)). Note its power density is almost equal to that of an equivalent turbine engine.

One point is shown (at 50,000 hp, 2600 lb) for a preliminary design of an LH_2-cooled synchronous machine (ref. 15). This cryogenic machine approaches being light enough to power a transport-sized aircraft, being about half the weight of an equivalent turbofan engine. This leaves some room for the weight of other components (electric power source and power conditioning), if they are acceptably light.

The switched reluctance motor point on the graph at 20 hp and 18 lb electromagnetic weight represents the initial tests on a NASA Glenn Research Center switched reluctance motor. This liquid-nitrogen-cooled machine has been operated with available low-power electric drives and is expected to reach several times its present specific power with upgraded power electronics. It is discussed further below.

Not shown in figure 7(c) is any data on power conditioning electronics. A major need is the development of power electronics that are much lighter due to utilization of cooling available from on-board cryogens.

Gearbox Weight

Data on existing and projected gearbox weights were gathered to let us evaluate whether a gearbox can be used between a motor and a propulsor. If the gearbox is light enough, the motor speed need not be constrained by the propulsor speed. The weights versus power outputs for these gearboxes are shown in figure 8.

A correlation that fits all the data rather well is shown in figure 9. Surprisingly, a single correlation reasonably fits both helicopter and fixed wing gearboxes, even though the output stage for helicopters must support very high torque. Curves appropriate for 1980, 2000 and future technology are shown. This correlation was used to derive the line in figure 7(c) for gearboxes, with the value of K chosen for year 2000 technology).

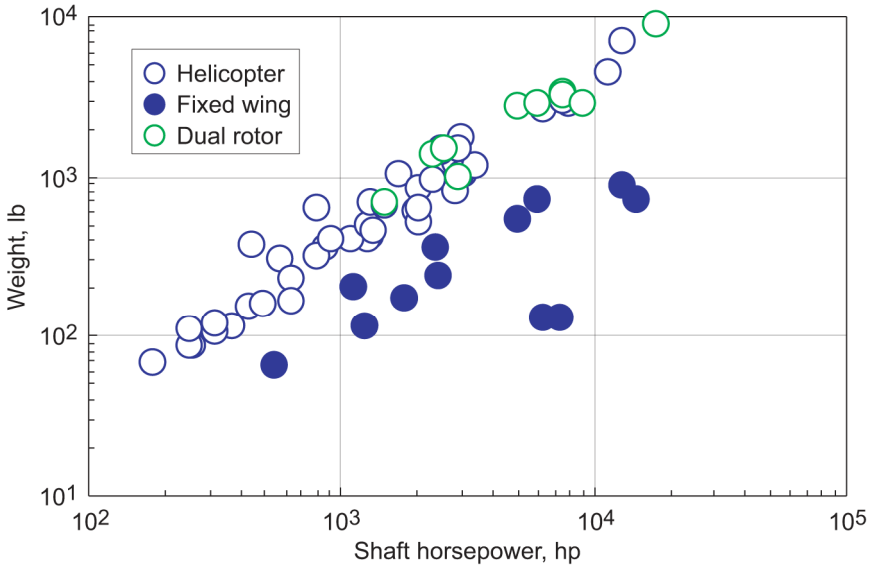

Figure 8.—Weight versus output shaft power for helicopter and fixed-wing gearboxes.

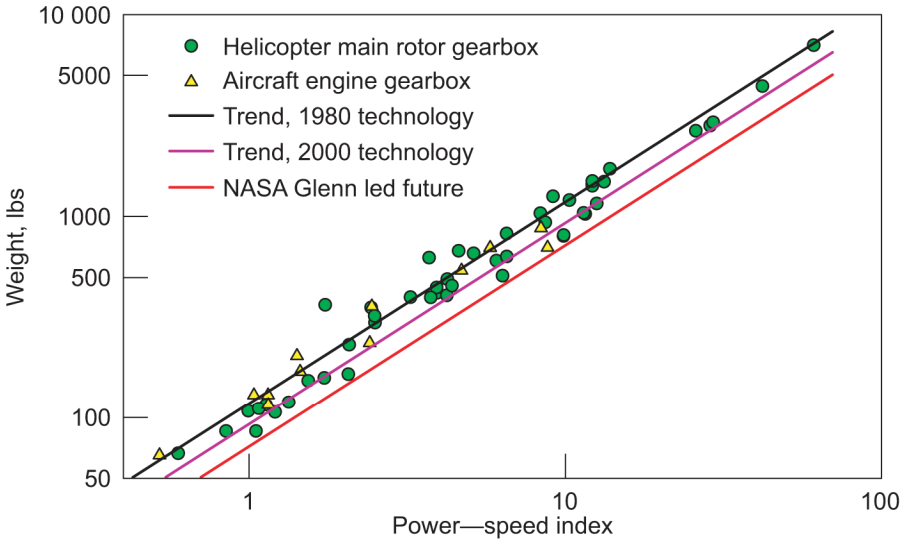

Index = $(hp)^{0.76} \bullet (\text{engine rpm})^{0.13}/(\text{rotor rpm})^{0.89}$

Weight = index • K where

K = 118 (year 1980)

= 94 (year 2000)

= 72 (future)

Figure 9.—Correlation of gearbox weights, including both helicopter and fixed wing boxes. Trend-lines: older technology—black, year 2000 technology—purple, and projected technology—red.

NASA Glenn In-House Program

The elements of our current program to advance high-power-density motors specifically for aircraft propulsion are shown in table II. Each of these is discussed in the subsections below.

TABLE II.—ELEMENTS OF NASA GLENN PROGRAM IN HIGH-POWER-DENSITY MOTORS

	Performing Organization	Type	Status
Cryogenic (non-superconducting) motor in liquid nitrogen	NASA GRC	--	Testing
Tip-Drive Permanent-Magnet Motor	NASA GRC	--	Build-up
Superconducting Synchronous Motor	NASA GRC	--	In Fabrication
Systems Analysis of Heavy, Efficient Drives	NASA GRC	--	In-Progress
450 hp Superconducting Motor in Liquid Hydrogen	Long Electromagnetics, Inc.	NRA	In-Progress
Optimized Motors with Novel Conductor	Pennsylvania State University	NRA	In-Progress
MgB2 Superconducting Coils for Synchronous Motors	Hyper Tech Research, Inc.	SBIR	In-Progress

Cryogenic (Non-Superconducting) Motor

The switched reluctance motor or generator is rugged, very fault tolerant and has a good power density (refs. 16 and 17). As noted above, reference 14 reports achieving nearly 5 hp per pound of electromagnetic weight (~8 kW/kg), or 3 hp/lb (5 kW/kg) of total weight, if total weight is 1.5 times electromagnetic weight. The switched reluctance motor can be operated well into saturation of its iron core and can produce substantial extra torque after saturation occurs in parts of its poles. With cryogenic cooling of the coils, operation far into saturation is possible.

We have designed and built a cryogenic switched reluctance motor that, in liquid nitrogen (LN_2), can sustain current densities in its coils of over 50 A/mm^2 steady current, or 70 A/mm^2 at a 50 percent duty cycle). This is 5 to 10 times the current density typically achieved in room temperature motor coils and about 6 times the level at which saturation sets in at pole alignment in our motor. This extra current density capability is due to the lower conductor resistance at liquid nitrogen (LN_2) temperature, the good heat transfer of nucleate boiling of the nitrogen and to specially designed coils that expose extra surface area to the LN_2. The high current density results in high torque and, with appropriate power conditioning, to high power at high speed. The rugged rotor (without coils or permanent magnets) permits high speed operation, as far as mechanical stress is concerned.

LN_2 may never be used in an actual application. Liquid hydrogen (LH_2) would reduce the conductor resistance by a further factor of 15 or more, but with some reduction in peak nucleate boiling heat flux from the coils. (See ref (18) for nucleate and film boiling data and correlations for LN_2 and LH_2.) The peak nucleate boiling heat flux for LN_2 is about 20 W/cm^2 and for LH2 about 10 W/cm^2. The minimum film boiling heat flux is very similar for both fluids, at slightly less than 1 W/cm^2. Thus we might expect the attainable coil current density to increase by a factor of $\sqrt{(15/2)} \approx 2.7$ in LH_2. However, we can validate all our analysis models by experiments in LN_2 at significantly less cost without adding LH_2 infrastructure to our laboratory. Furthermore the motor can serve as a test-bed for improving coil geometries just as well in LN_2 as in LH_2.

The elements of our cryogenic switched-reluctance motor program are shown in table III.

TABLE III.

- Conductor current capacity measurements
- Higher current from coil configuration improvements
- Finite element calculations of torque
- Locked-rotor torque measurements
- Back EMF measurements
- Flux linkage measurements
- Torque and power measurements
- Extension to higher power with power electronics upgrade

The cryogenic switched reluctance motor is the farthest along of the motors in our development program, so some of our experimental results are presented.

Coil Current-Carrying Capacity

Current carrying capacity results for three types of coils for the motor are shown in figure 10. Photographs of the coils are shown in figure 11. Two of the 80-turn, 4-layer coils (number 18 magnet wire) have end turns configured like heat exchangers, spaced apart to provide greater heat transfer area to dissipate the ohmic heating from the coil. Such coils might be called "self-finned". The number of turns was chosen to match the current capacity of the initially available power conditioning and will have to be greatly reduced to reach the motor's maximum power potential. The bodies of the coils are epoxy-impregnated, but no epoxy is applied to spaced end turns. In the close-packed coil, heat generated internally must be conducted partially through copper and partially through epoxy to reach the LN_2-cooled surface. Most of the thermal drop occurs in the epoxy. In the coils with spaced end turns, the majority of the heat generated in the mid regions of the coil is conducted to the end turns, and dissipated from the large exposed surface.

The room-temperature voltage-versus-current measurements in figure 10 show a thermal runaway condition beginning at about 6 to 8 A. The curves shown for the coils immersed in an LN_2 bath (not mounted in the motor) show an initial slope (resistance) of $1/7^{th}$ of the room temperature value. The approach to thermal runaway begins at much higher currents: around 50 A for the tight-wound coil, around 65 A for the coil with semi-spaced ends and above 70 A for the coil with fully spaced ends.

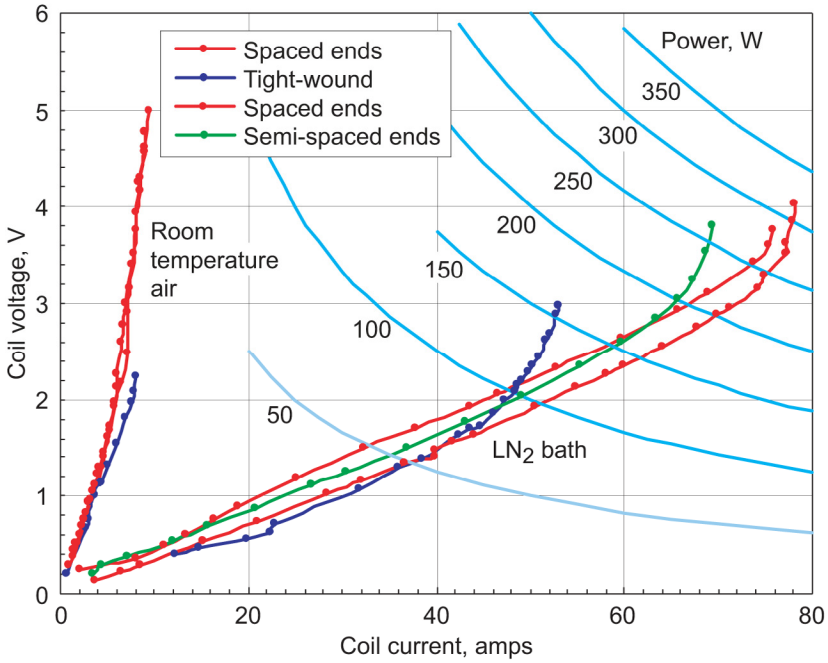

Figure 10.—Coil voltage drop versus coil current (steady direct current) at room temperature and in LN_2 bath for three coil configurations.

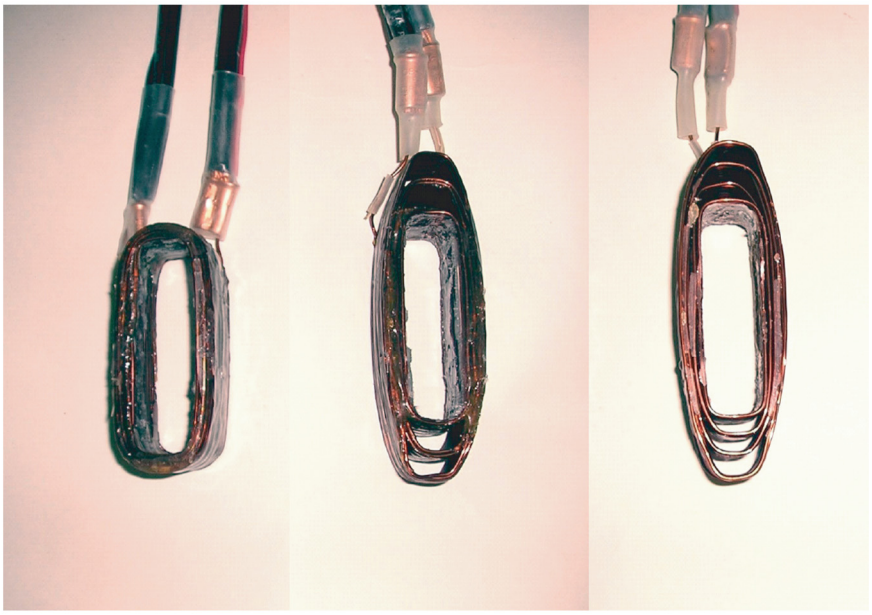

Figure 11.—Left to right: Conventional tight-wound (close-packed) coil, coil with partially-spaced end turns and coil with fully-spaced end turns.

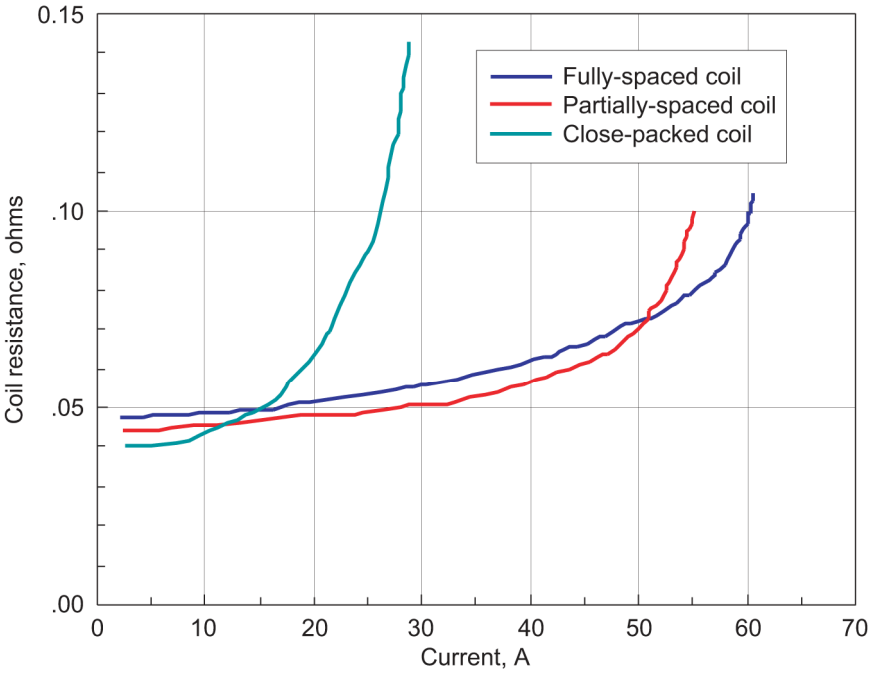

Figure 12.—Resistance versus current for coils installed in motor in LN_2. Note the current is steady direct current (the worst case for heat generation).

Mounted in the more confined slots of the motor, the coils are not as well cooled by LN_2. Measurements of coil resistance installed in the motor in liquid nitrogen are shown in figure 12. The close-packed coil loses nearly half of its area exposed to liquid nitrogen when in the motor and begins to heat substantially above 20 A. The coils with fully spaced end turns are usable to 50 A or more. Note that this gives a current density in the motor slots of ≥50 A/mm^2 if the coils are wound with 100 percent dense square packing. Note that this is not far below the 63 A/mm^2 reported for superconducting rotor coils operating at 27 K (ref. 19). However, it must be noted that the rotor application is much more difficult

structurally and thermally than our stator application. All currents discussed so far have been steady direct currents. The ideal current wave form in actual motor operation is approximately rectangular at roughly a 50 percent duty cycle for maximum torque or 33 percent for minimum torque ripple. Hence the maximum current during motor operation could be either √2 times as much, or about 70 A for maximum torque or √3 times as much, or nearly 90 A for minimum torque ripple.

These measurements show the benefits of both the reduction in resistance due to the low temperature and the excellent nucleate boiling heat transfer environment, as well as the benefit of configuring the coils for maximum heat dissipation. Such high currents allow utilization of the switched reluctance motor's ability to produce extra torque far into the magnetic saturation, as will be seen below.

Motor Hardware

The motor is a 12/8 configuration—twelve stator poles and eight rotor poles. It therefore has three independent phases. The stator O.D. is 7.25 in (18.4 cm); the rotor O.D. is 3.96 in (10.1 cm) and the axial length of the lamination stack is 1.97 in (5.08 cm). The radial air gap is 20 mils (0.051 cm). The stator-pole arc, the stator-pole-gap arc and the rotor-pole arc are all equal. The laminations are 6 Mils (0.152 mm) thick and are made of 49 percent Co, 49 percent Fe and 2 percent V. (Hiperco 50 HS). A photograph of the stator with one coil installed is shown in figure 13.

Figure 14 shows a photograph of the motor, mounted with a vertical axis to simplify submersion in LN_2, with six of its twelve coils installed. For simplicity the entire motor is submerged in LN_2, not just the coils. This has the obvious disadvantage of considerable drag due to the rotor churning the LN_2. Fortunately, LN_2 has a relatively low viscosity. Liquid nitrogen viscosity is about 15 percent of that of water at room temperature. For this proof-of-principle test article, we avoided the complication of designing the motor so that LN_2 bathes only the stator.

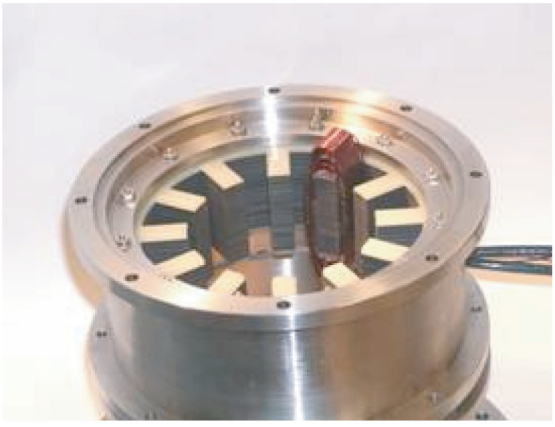

Figure 13.—Twelve-pole stator with one coil installed.

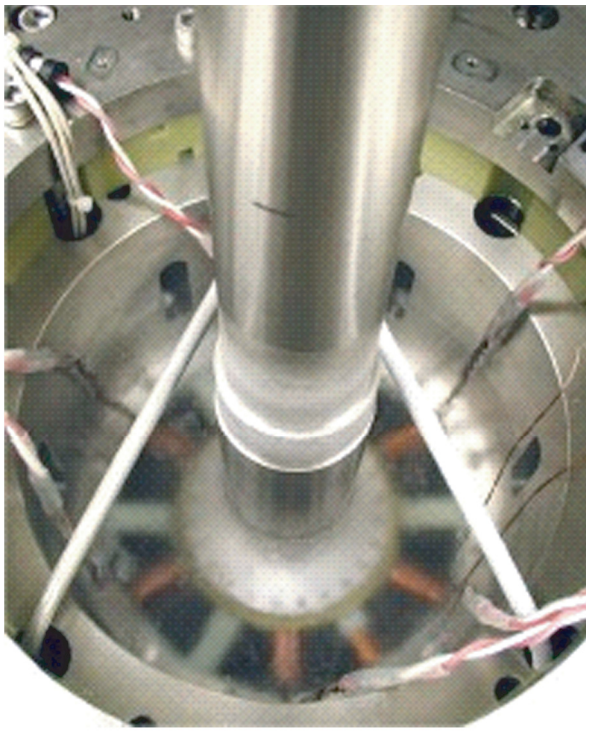

Figure 14.—Switched reluctance motor submerged in LN_2. The coils appear hazy because they are seen through the liquid. Frost is visible on the shaft and other parts.

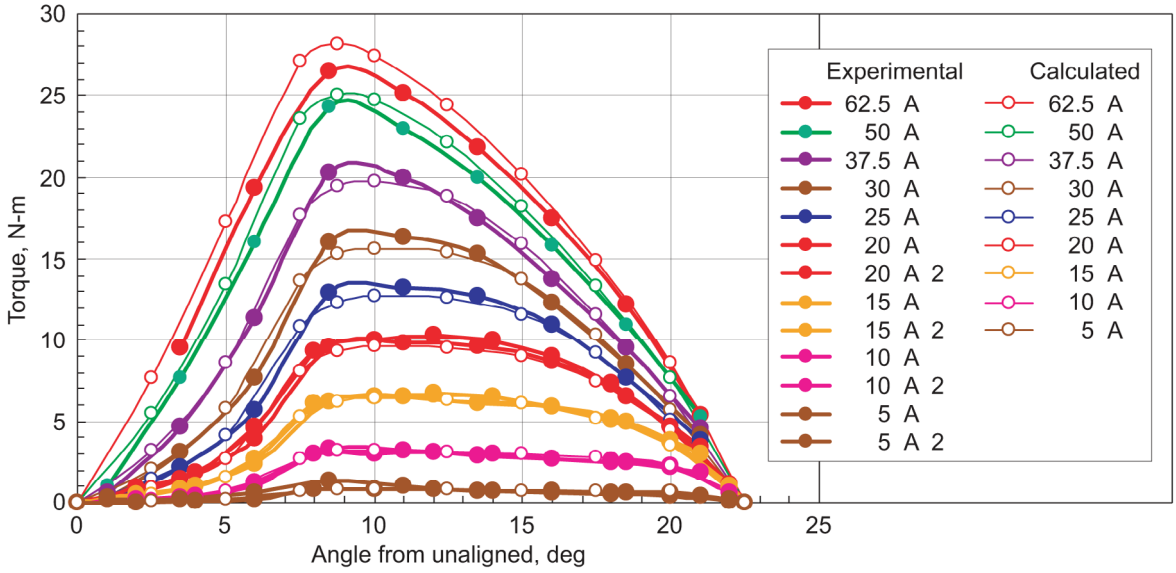

Figure 15.—Calculated and experimental torque for two opposite poles energized in the switched-reluctance motor. Experimental curves have solid symbols; calculated curves have open symbols and are de-rated (reduced) by 12%.

Calculated and Experimental Locked-Rotor Torque

Finite element (F.E.) predictions of the locked-rotor torque were made using a commercial 2-D F.E. code (Maxwell 2D) for several values of rotor angle from unaligned to aligned and for five values of coil current. Both the calculations and experiments were for two opposite poles energized. Experimental locked-rotor torque was measured by using a lever arm, mounted on the rotor, which pressed on a load cell. Multiplying the F.E. code results by a "de-rating" factor of 88 percent (chosen somewhat arbitrarily) gives rough, but by no means uniform, agreement between calculated and measured torque, as seen in figure 15. Note that the qualitative shape of the curves is reasonably matched.

It is beyond the scope and intent of this effort to try to determine or recommend a de-rating factor. But we do expect some de-rating to be required for three reasons. First, the actual length of our installed lamination stack was only 0.986 of the length assumed for the calculations. Secondly, the actual packing fraction of the laminations was 0.968, versus perfect packing assumed in the calculation. And thirdly and most importantly, the 2-D finite element calculations cannot take axial fringing of flux into account. (A fourth possibility would arise if the material B-H curve were for laminations not insulated with oxide. An oxide coating effectively reduces the packing fraction of the core. But we used data for 0.004 in. thick laminations with an oxide coating, and our actual laminations are 0.006 in. thick oxide coated. So we have, in effect done calculations based on a material with more oxide than we actually have.) We expect the fringing to become worse at higher currents, giving an increasing over-prediction of torque as exciting current rises. Indeed one can see from figure 15 that better agreement between experiment and calculation could be obtained with a smaller reduction of the calculated torque for low currents and a larger reduction for high currents.

Running Torque and Power

The motor has been run at 16,000 rpm at room temperature for short periods of time (on the order of 15 to 20 seconds), without undue heating. It has run at various speeds up to 11,000 rpm in liquid nitrogen for longer periods.

Torque and power outputs were measured at room temperature and in liquid nitrogen. Because a dynamometer was not available for the tests, torque and power were derived from the speed as a function of time during a fast acceleration. One pulse-width-modulated power amplifier under PC control was used to power each of the 12 coils. Running in current mode, power amplifiers supplied up to 30 A peak current at up to 158 V. These peak values are much too low to approach the full torque and power potential of this motor, but were the best available for the initial tests.

A typical speed-versus-time record for an acceleration test is shown in figure 16. The motor accelerates with no load, except its own inertia, friction and windage, from an 880 rpm idle to 8000 rpm in approximately 0.25 sec. Torque T and power P are found as functions of time from $T = I_p \, d\Omega/dt$ and $P = T \, \Omega$, where Ω is shaft speed and I_p (0.0048 kg-m^2) is the polar moment of inertia.

The maximum output torque achieved to date was 23.7 N-m at approximately 2700 rpm for 30 A maximum current. An upper bound for the low-speed torque, for optimum firing and commutation angles, can be derived by averaging locked-rotor torque from figure 15 over angle and projecting to 12 coils. The result for 30 A current is 28 N-m. We have achieved 85 percent of that locked rotor torque while running at low speed. Note that bearing friction and windage torques should be added to the observed net output torque for comparison to the locked-rotor torque. Further use of figure 15 data indicates that about 60 N-m low-speed torque should be obtainable at current levels shown feasible in figure 12.

The maximum power output achieved for 30 A maximum current and 158 V was 13 hp (9.7 kW), which occurred at approximately 4900 rpm. The low-speed torque could be extended to much higher speed by a combination of fewer turns (hence higher current) and higher applied voltage. Planned upgrades of the power conditioning should permit an order of magnitude increase in power output. Figure 17 shows upper bounds for the power that would be produced at speeds up to 30,000 rpm (the rotor safe-speed limit from stress analysis) at two values of torque, 23.7 N-m (which has been produced) and 60 N-m (which is indicated possible at current densities achieved in static tests). Many factors will likely prevent achieving these upper-bound projected power levels, especially coil voltage limits, but also including controller sample rate and power converter switching rate, large electrical leads to the motor, conductor skin effect, LN_2 use rate, LN_2 pumping and sloshing, rotor and stator eddy currents and back-iron saturation.

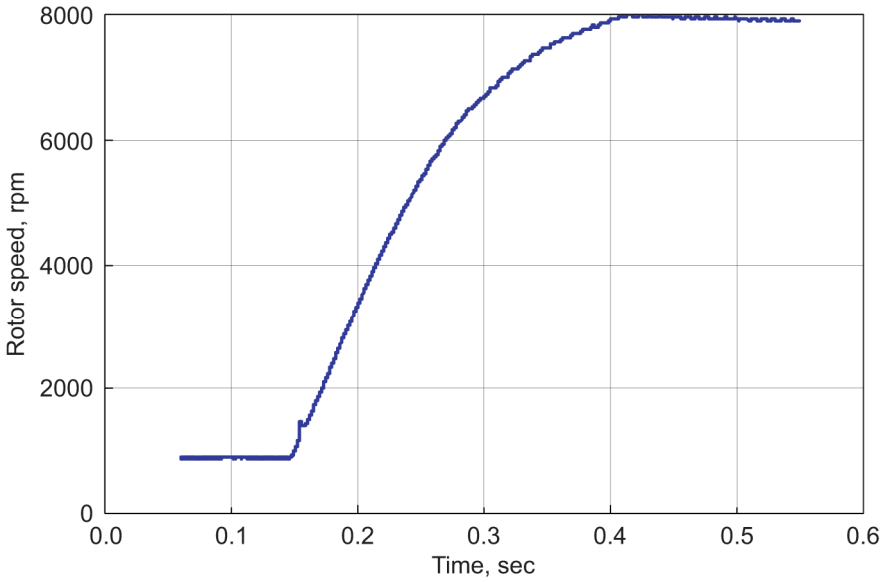

Figure 16.—Speed as a function of time for a fast acceleration.

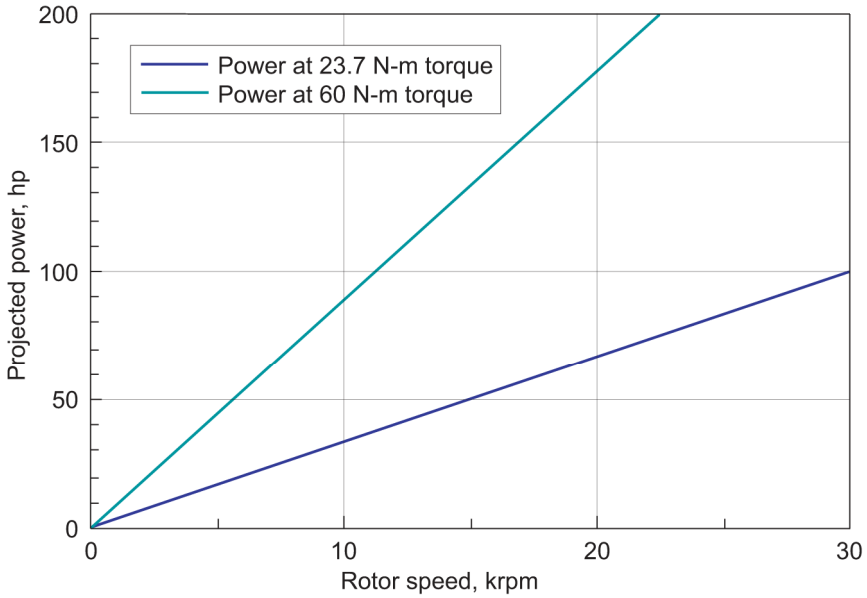

Figure 17.—Projected power. The lower line is based on running torque already produced. The upper line is based on the running torque expected to be achieved at current densities that have already been achieved in static tests.

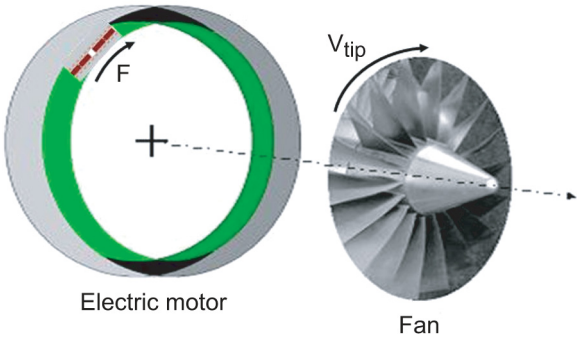

Figure 18.—Tip-drive motor to fit around propulsive fan.

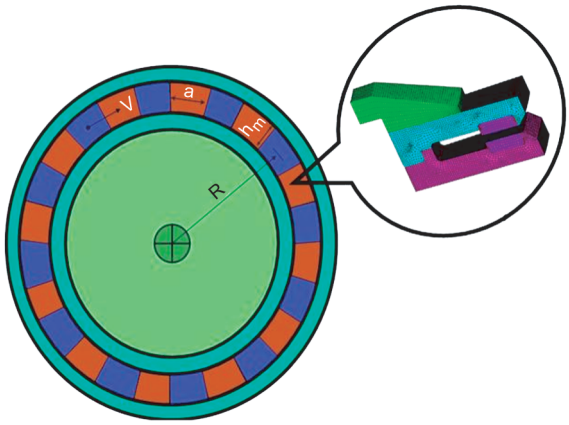

Figure 19.—Rotor permanent magnet arrangement for tip-drive motor.

Tip Drive Motor

A scaled blade-tip-drive test rig was designed and is being assembled. The rig is a scaled version of a DC brush-less motor which would be located in the shroud of a thrust fan, figure 18. This geometry is very attractive since the allowable speed of the armature is approximately the speed of the blade tips, (Mach 1 or 1100 ft/s). The magnetic pressure generated in the motor acts over a large area; and thus, produces a large force or torque. In addition, it has a large area to remove heat. This force multiplied by the large velocity results in a high power density motor. The downside is that this design results in large stresses on the rotating components.

The concept being studied has rotating back-iron and segmented permanent magnets, figure 19. The back-iron acts as structural support for the rotating magnets and also as a return path for the magnetic flux. The magnetic flux is fixed with the rotating back-iron and thus does not produce any eddy currents. The stator is between the permanent magnets and its coupling with the back-iron is minimized to result in a low inductance. This increases the response of the switched current in each phase.

The goal of the test program is to maximize both the armature speed and the stator current density, thus producing a very high power density motor. The unique feature of the rig, (fig. 20), is that a test generator provides the electrical current and voltage to drive a test motor. The test motor and an auxiliary motor provide the torque to drive the generator. The auxiliary motor will also control the speed of the test rig. Later a PWM motor drive will be developed to drive the motor and the torque will be absorbed by the generator.

An assembled view of the rig is shown in figure 21. The auxiliary motor drives the test motor-generator through a pulley. The test motor- generator is supported on oil mist lubricated ball bearings, with a rub bearing backing up the ball bearings. The voltage difference between the test generator and the test motor is controlled by shims in the air gaps between the permanent magnets. The inductance of the test motor-generator is very low and most of the losses should be resistive losses in the stator wires.

A small stationary test rig, shown in figure 22, was designed and is being assembled to test various stator cooling techniques. The objective is to improve the current density and thus the power density of the motor. Examples of cooling concepts to be investigated are edge cooling, surface cooling, etc. The permanent magnets are arranged north-south-north-south-etc.; and a back-iron is used outside of the magnets to form a return path. Each phase of square Litz-wire goes down one pole and up the adjacent pole. The stator wiring between the magnets is compressed tightly into a thin, flat shape with epoxy and fiberglass to maintain its plate-like structure. The stator moves relative to a fixed holder. The force and displacement, due to the current flow in the stator wiring, will be measured at the fixed holder end.

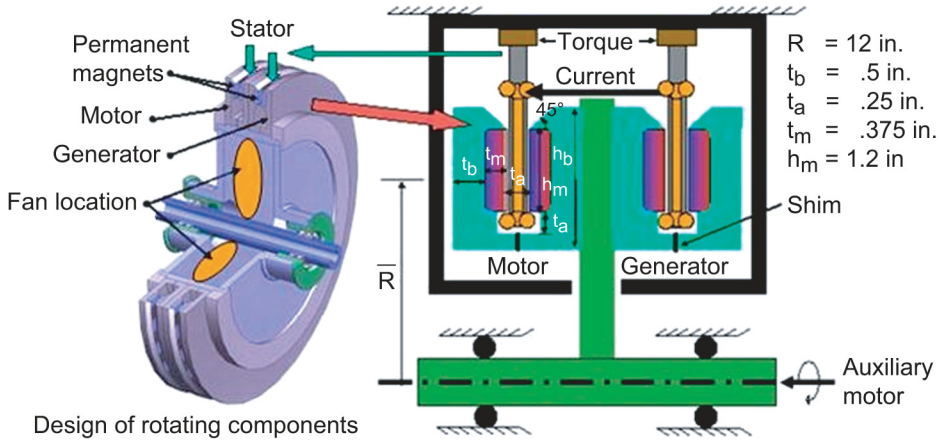

Scaled blade tip drive test rig

Power = 115 kW, Voltage = 576 V, Current = 50 A/phase, Phases = 4,
Tip speed = 1000 ft/s, Torque = 85 ft-lb, Speed = 9550 rpm

Figure 20.—Motor and generator sharing a common shaft.

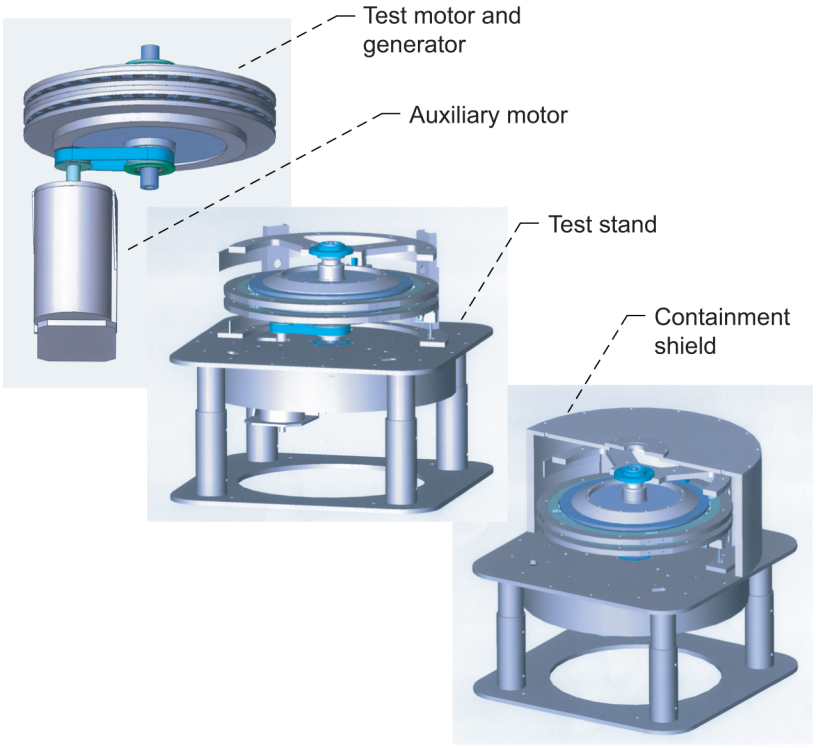

Figure 21.—Assembled view of tip-drive rig.

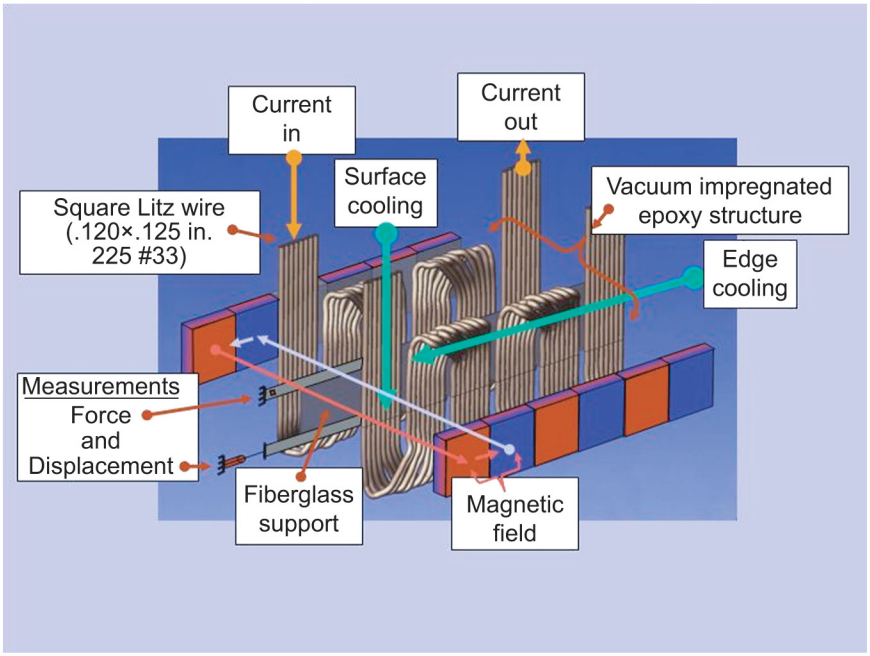

Figure 22.—Test section of tip-drive motor.

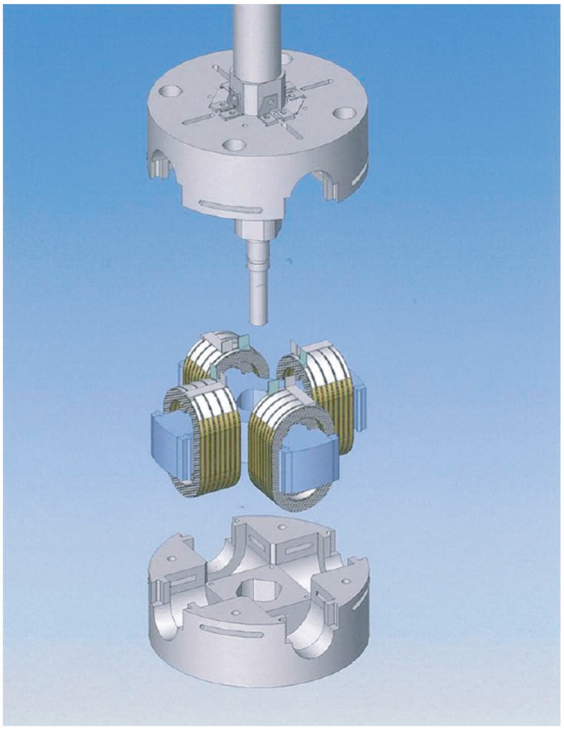

Figure 23.—Exploded drawing of the four-pole rotor and the containment parts that restrain it.

High Temperature Superconducting Motor

A four-pole synchronous motor with high-temperature-superconducting DC rotor windings and a standard three-phase AC stator has been designed and detailed for fabrication for a test bed facility. The motor will be operated in LN_2 and possibly later in LH_2. Initially the rotor windings will be commercially available BSSCO superconductor, which has only modest current-carrying capacity at LN_2 temperature in an applied field of a few tenths of a Tesla. Hence the first version will have an iron core and field-reducing "feet" at the ends of the rotor poles. When YBCO superconductor is available, the coils will be replaced with ones wound with that conductor and the iron core may be replaced with a non-magnetic core. Possible testing in liquid hydrogen is being considered.

The motor is designed to run to approximately 6000 rpm. Its rotor coils will be tape-wound and race-track shaped. The stator will be wound with copper conductor. Both rotor and stator coils will be cooled by LN_2. An exploded drawing of some rotor parts is shown in figure 23.

System Analysis of Heavy, Efficient Drive

As noted previously, fuel cells appear to be too heavy to use as the power source for transport-size aircraft. However, they will likely be much more efficient than turbine engines. Similarly, the turbo-generator-motor drive system for a propulsor will likely be heavier than a straight turbine drive, because of the extra components. However, the turbo-generator-motor drive system may be more efficient than direct drive because the turbine main shaft is not constrained to the low speed of the propulsor and other factors. Because a more efficient system requires less fuel, higher weight can be offset to some degree. We are doing a preliminary system study to see how much heavier a candidate propulsor drive system can be for a given efficiency improvement yet still use the same amount of fuel. Any further efficiency improvement of the candidate system would save fuel, in spite of the heavier power plant.

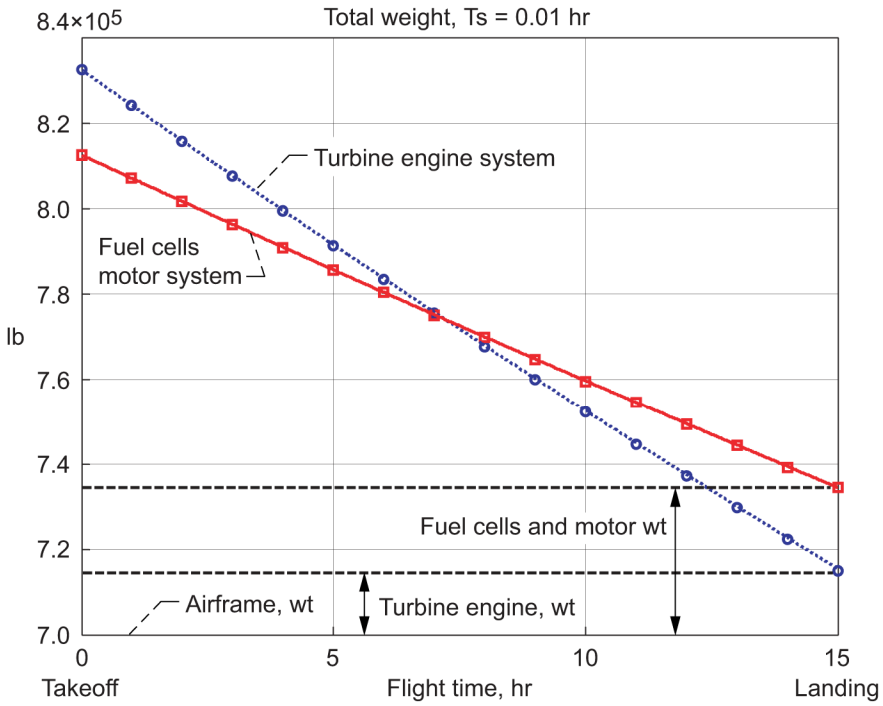

Figure 24.—Aircraft weight as a function of time during flight for baseline system (40% efficient) and a fuel-cell powered system (assumed 60% efficient).

For an initial simplified comparative study, we assumed both power plants are liquid hydrogen (LH_2) fueled, and the Boeing 747-400 airframe and its characteristics were used for both systems. We ignored increased tankage weight or changes in airframe shape required to accommodate LH_2. The simulation model, which consists of takeoff, climb, cruise, and landing modules, was developed using specifications and characteristics obtained from the aircraft and engine manufactures, internet websites, and other published sources. The CF6-80C2 engine that provides up to 63,500 lb of thrust at sea level and a range of approximately 8,400 statute miles (13,520 km) was chosen for the simulation model.

Electric drive train components (fuel cells, power conditioning and motors) were characterized by simple specific-power coefficients and efficiencies. The Power Specific Fuel Consumption (SFC, lb/hr/hp) and aircraft range were calculated.

Figure 24 shows one example of the simulation results for total aircraft weight, as a function of time during flight, for the baseline turbine-powered system and a fuel-cell-motor-powered system from takeoff to landing during a 15-hr flight. As seen from the figure the fuel-cell-powered aircraft uses less fuel even though it is much heavier than the turbine-engine-powered aircraft. The heavier, more efficient system looks better for long flights, poorer for short ones.

450 hp Liquid-Hydrogen-Cooled Superconducting Motor

Sized to power a general aviation aircraft, a 450 hp wound-rotor synchronous motor is being designed and will be built by Long Electromagnetics Inc. (ref. 15 and 20). The motor will use technology similar to what would be used to power transport-sized aircraft, but will be greatly scaled down. Its rotor will have 4 salient poles, wound with replaceable combinations of BSSCO superconductor and copper coils and possibly some MgB_2 coils. The stator will be a standard three-phase AC stator with copper windings. Both rotor and stator will be cooled by LH_2. The motor will run at about 6000 rpm. Initially the rotor current will be supplied through slip rings. The motor is intended to serve as a test bed for various types

of rotor and stator conductors, as well as for testing power sources and power conditioning electronics. With some modifications, it could actually be used as an early electric flight demonstration unit.

Optimized Motors With Novel Conductor

During Phase I of an NRA contract, Pennsylvania State University developed two-dimensional electromagnetic and structural continuum models to optimize ultrahigh-power density machines and evaluated performance envelopes of machine designs constructed using various electromagnetic and structural materials. In the Phase II contract (ref. 21), in progress at this writing, the coupled thermal, structural, and electromagnetic problem will be solved to include mechanical and thermal considerations, including the nonlinear, coupled constitutive properties of high-purity aluminum, implicit in the assumption of high current density. In addition, the manufacturing process using high purity aluminum and composite material will be investigated to minimize resistivity increases due to manufacturing-induced strains as well as operation-induced strains. Experimental tests will be conducted to determine the thermal, structural, and electrical properties of this structure at cryogenic temperatures. There is at present no commercial source of high purity aluminum conductor suitable for cryogenic motors.

MgB_2 Superconducting Coils for Synchronous Motors

Magnesium diboride (MgB_2) is possibly the lowest-cost and lightest superconductor that might be used in wound rotors of synchronous motors cooled by LH_2. Under a Phase II SBIR contract (ref. 22), conductor and test coils will be produced that can be used in a motor like the 450 hp motor mentioned above.

Concluding Remarks

The benefits of electric drive that have been exploited in trains and ships may be extended to hydrogen-fueled aircraft. Cryogenic motors with either pure normal conductors or superconductors can likely produce the required specific power. Advanced designs of room-temperature motors will produce sufficient specific power density for smaller aircraft. Electric motor power densities greater than those of turbine engines are easily possible.

The NASA GRC in-house program in this area is constructing and testing sub-scale models of several candidate motor types: switched reluctance (in testing), axial-gap permanent magnet (under construction) and superconducting synchronous (designed). Contracts support the development and construction of a motor large enough to power a general-aviation-sized aircraft, optimization studies to explore the limits of synchronous motor power density, the development of a novel composite conductor and the development of an MgB_2 conductor suitable for synchronous motor rotors. Yet unexplored are ways to utilize cryogenic cooling to reduce the weight of power conditioning electronics.

References

1. Gerald V. Brown and Willard D. Coles, High-Field Liquid-Neon-Cooled Electromagnets, Cryogenic Engineering Conference, Houston, TX, Aug. 23–25, 1965.
2. J.C. Laurence, G.V. Brown, Jacob Geist, and Kenneth Zeitz, “A Large Liquid-Neon-Cooled Electromagnet,” High Magnetic Fields, (Proceedings of the International Conference on High Magnetic Fields, Cambridge, MA, 1–4 Nov. 1961), ed. H. Kolm, B. Lax, F. Bitter and R. Mills, Wiley & Sons, New York, (1962) 170–179.
3. C.E. Oberly and J.C. Ho, The Origin and Future of Composite Aluminum Conductors, IEEE Transactions on Magnetics, vol. 27, no. 1, Jan. 1991.

4. A.P. Malozemoff, W. Carter, S. Fleshler, et al., "HTS Wire at Commercial Performance Levels," IEEE Trans. Appl. Superconductivity, vol. 9, no. 2, June 1999.
5. American Super Conductor website, http://www.amsuper.com/products/htsWire/documents/4122GWhitePaper_v5.pdf
6. Gus Khalil, TACOM: http://www.tacom.army.mil/tardec/electric_drive/motors
7. Charles E. Oberly, AFOSR/AFRL Propulsion Directorate, Power Division, Power Generation Branch, WPAFB, private communication.
8. Jane's Aero-Engines, Edited by Bill Gunston OBE, FRAes, Jane's Information Group Inc., Copyright 2000, ISBN 0 7106 1405 5, http://www.janes.com.
9. Jane's Aero-Engines, Edited by Bill Gunston OBE, FRAes, Jane's Information Group Inc., issue 15, March 2004, Copyright 2004, ISBN 0 7106 1405 5, http://www.jae.janes.com .
10. Jane's All The World's Aircraft, Editor-in-Chief: Paul Jackson, MRAeS, Deputy Editor: Kenneth Munson, AMRAeS, Assistant Editor: Lindsay Peacock, Ninety-fourth year of issue 2003–2004, Jane's Information Group Inc., Copyright 2003, ISBN 0 7106 2537 5, http://www.jawa.janes.com
11. The Engine Handbook, Propulsion Product Group Manager, San Antonio Air Logistics Center, Kelly Air Force Base, Texas, 1995 Edition.
12. Jeffrey J. Berton, Joshua E. Freeh, and Timothy J. Wickenheiser, "An Analytical Performance Assessment of a Fuel Cell-Powered, Small Electric Airplane," NASA/TM—2003-212393, Prepared for the Symposium on Novel and Emerging Vehicle and Vehicle Technology Concepts, organized by the Applied Vehicle Technology Panel of the North Atlantic Treaty Organization Research and Technology Agency, Brussels, Belgium, April 7–11, 2003.
13. Ferreira, C.A., Jones, S.R., Heglund, W.S., and Jones, W.D., "Detailed Design of a 30-kW Switched Reluctance Starter/Generator System for a Gas Turbine Engine Application," IEEE Ind. Appl., vol. 31, issue 3, pp. 55–561 (1995).
14. Arthur V. Radun, High-Power Density Switched Reluctance Motor Drive for Aerospace Applications," IEEE Transactions on Industry Applications, vol. 28, no. 1, Jan./Feb. 1992.
15. Final Report, Phase I NRA Contract NAS3 02112, "Design of Lightweight High Power Motors and Generators for Electric Aircraft Propulsion," Long Electromagnetics, Inc, 700 Technology Drive, Room 5107, Pittsburgh, PA 15219; Larry Long, P.I.; Albert F. Kascak, Technical Monitor. March 31, 2003.
16. T.J.E. Miller, Switched Reluctance Motors and Their Control, Magna Physics Publishing and Clarendon Press, Oxford, 1993.
17. Rama Krishnan, Switched Reluctance Motor Drives, CRC Press, Boca Raton, FL, 2001.
18. E.G. Brentari and R.V. Smith, "Nucleate and Film Pool Boiling Design Correlations for O_2, N_2, H_2, and He," vol. 10, pp. 325–341, International Advances in Cryogenic Engineering, Proceedings of the 1964 Cryogenic Engineering Conference, K.D. Timmerhaus, Ed, Plenum Press, New York, 1965.
19. J.P. Voccio, B.B. Gamble, C.B. Prum, and H.J. Picard, 125 HP HTS Motor Field Winding Development, IEEE Transactions on Applied Superconductivity, vol. 7, no. 2, pp. 519–522, June 1997.
20. Phase II NRA Contract, NAS3–03106, Long Electromagnetics Inc., Larry Long, P.I., 700 Technology Drive, Room 5107, Pittsburgh, PA 15219, Albert F. Kascak, Technical Monitor.
21. Phase II NRA Contract, NAG3–03101, Pennsylvania State University, Prof. Heath Hofmann and Prof. Charles Bakis, P.I.'s, 110 Technology Center, 200 Innovation Blvd., University Park, PA 16802, Jeffrey J. Trudell, Technical Monitor.
22. Phase II SBIR Contract No. NNC05CA04A, Hyper Tech Research Inc., Dr. Mike Tomsic, P.I., 110 E. Canal St., Troy, OH, 45373, Jeffrey J. Trudell, Technical Monitor, Dec. 1, 2004

REPORT DOCUMENTATION PAGE

Form Approved
OMB No. 0704-0188

1. AGENCY USE ONLY (*Leave blank*)	2. REPORT DATE	3. REPORT TYPE AND DATES COVERED
	December 2005	Technical Memorandum

4. TITLE AND SUBTITLE

NASA Glenn Research Center Program in High Power Density Motors for Aeropropulsion

5. FUNDING NUMBERS

WBS–22–066–30–02
1L161102AF20

6. AUTHOR(S)

Gerald V. Brown, Albert F. Kascak, Ben Ebihara, Dexter Johnson, Benjamin Choi, Mark Siebert, and Carl Buccieri

7. PERFORMING ORGANIZATION NAME(S) AND ADDRESS(ES)

National Aeronautics and Space Administration
John H. Glenn Research Center at Lewis Field
Cleveland, Ohio 44135–3191

8. PERFORMING ORGANIZATION REPORT NUMBER

E–15158

9. SPONSORING/MONITORING AGENCY NAME(S) AND ADDRESS(ES)

National Aeronautics and Space Administration
Washington, DC 20546–0001
and
U.S. Army Research Laboratory
Adelphi, Maryland 20783–1145

10. SPONSORING/MONITORING AGENCY REPORT NUMBER

NASA TM—2005–213800
ARL–MR–0628

11. SUPPLEMENTARY NOTES

Gerald V. Brown, Dexter Johnson, and Benjamin Choi, NASA Glenn Research Center; Albert F. Kascak, U.S. Army Research Laboratory, NASA Glenn Research Center; Ben Ebihara, Mark Siebert, and Carl Buccieri, University of Toledo, 2801 W. Bancroft Street, Toledo, Ohio 43606–3390. Responsible person, Gerald V. Brown, organization code RSS, 216–433–6047.

12a. DISTRIBUTION/AVAILABILITY STATEMENT

Unclassified - Unlimited
Subject Category: 07

Available electronically at http://gltrs.grc.nasa.gov

This publication is available from the NASA Center for AeroSpace Information, 301–621–0390.

12b. DISTRIBUTION CODE

13. ABSTRACT ***(Maximum 200 words)***

Electric drive of transport-sized aircraft propulsors, with electric power generated by fuel cells or turbo-generators, will require electric motors with much higher power density than conventional room-temperature machines. Cryogenic cooling of the motor windings by the liquid hydrogen fuel offers a possible solution, enabling motors with higher power density than turbine engines. Some context on weights of various systems, which is required to assess the problem, is presented. This context includes a survey of turbine engine weights over a considerable size range, a correlation of gear box weights and some examples of conventional and advanced electric motor weights. The NASA Glenn Research Center program for high power density motors is outlined and some technical results to date are presented. These results include current densities of 5,000 A/cm^2 current density achieved in cryogenic coils, finite element predictions compared to measurements of torque production in a switched reluctance motor, and initial tests of a cryogenic switched reluctance motor.

14. SUBJECT TERMS

Aeropropulsion; High power density motors; Aircraft propulsion motors; Cryogenic motors; Superconducting motors; Switched reluctance motors;

15. NUMBER OF PAGES

27

16. PRICE CODE

17. SECURITY CLASSIFICATION OF REPORT	18. SECURITY CLASSIFICATION OF THIS PAGE	19. SECURITY CLASSIFICATION OF ABSTRACT	20. LIMITATION OF ABSTRACT
Unclassified	Unclassified	Unclassified	